Variations in Surface Air Temperature Observations in the Arctic, 1979–97

IGNATIUS G. RIGOR

Polar Science Center, Applied Physics Laboratory, University of Washington, Seattle, Washington

ROGER L. COLONY

International Arctic Research Center, University of Alaska, Fairbanks, Alaska

SEELYE MARTIN

School of Oceanography, University of Washington, Seattle, Washington

ABSTRACT

The statistics of surface air temperature observations obtained from buoys, manned drifting stations, and meteorological land stations in the Arctic during 1979–97 are analyzed. Although the basic statistics agree with what has been published in various climatologies, the seasonal correlation length scales between the observations are shorter than the annual correlation length scales, especially during summer when the inhomogeneity between the ice-covered ocean and the land is most apparent. During autumn, winter, and spring, the monthly mean correlation length scales are approximately constant at about 1000 km; during summer, the length scales are much shorter, that is, as low as 300 km. These revised scales are particularly important in the optimal interpolation of data on surface air temperature (SAT) and are used in the analysis of an improved SAT dataset called International Arctic Buoy Programme/Polar Exchange at the Sea Surface (IABP/POLES). Compared to observations from land stations and the Russian North Pole drift stations, the IABP/POLES dataset has higher correlations and lower rms errors than previous SAT fields and provides better temperature estimates, especially during summer in the marginal ice zones. In addition, the revised correlation length scales allow data taken at interior land stations to be included in the optimal interpretation analysis without introducing land biases to grid points over the ocean. The new analysis provides 12-h fields of air temperatures on a 100-km rectangular grid for all land and ocean areas of the Arctic region for the years 1979–97.

The IABP/POLES dataset is then used to study spatial and temporal variations in SAT. This dataset shows that on average melt begins in the marginal seas by the first week of June and advances rapidly over the Arctic Ocean, reaching the pole by 19 June, 2 weeks later. Freeze begins at the pole on 16 August, and the freeze isotherm advances more slowly than the melt isotherm. Freeze returns to the marginal seas a month later than at the pole, on 21 September. Near the North Pole, the melt season length is about 58 days, while near the margin, the melt season is about 100 days. A trend of $+1°C$ (decade)$^{-1}$ is found during winter in the eastern Arctic Ocean, but a trend of $-1°C$ (decade)$^{-1}$ is found in the western Arctic Ocean. During spring, almost the entire Arctic shows significant warming trends. In the eastern Arctic Ocean this warming is as much as $2°C$ (decade)$^{-1}$. The spring warming is associated with a trend toward a lengthening of the melt season in the eastern Arctic. The western Arctic, however, shows a slight shortening of the melt season. These changes in surface air temperature over the Arctic Ocean are related to the Arctic Oscillation, which accounts for more than half of the surface air temperature trends over Alaska, Eurasia, and the eastern Arctic Ocean but less than half in the western Arctic Ocean.

1. Introduction

Until recently the Arctic Ocean has lacked a systematic, accurate dataset on surface air temperature (SAT) at 2-m height. These data are especially important in the Arctic because most simulations by global climate models with enhanced greenhouse forcing predict that any warming in the global climate will be amplified at the poles. This implies that any change in the climate may first be detected at the poles. In addition, although the winter heat balance of multiyear ice is strongly dominated by the radiation balance, the ice growth in open water and leads is more strongly dominated by the sensible and latent heat fluxes, which depend strongly on the SAT. These SAT fields are essential for studies of climate change and for validation and forcing of numerical models.

Corresponding author address: Ignatius G. Rigor, Polar Science Center, Applied Physics Laboratory, University of Washington, 1013 NE 40th Street, Seattle, WA 98105.
E-mail: igr@apl.washington.edu

Martin and Muñoz (1997, hereafter referred to as MM) studied the accuracy of gridded temperature datasets from the National Center for Atmospheric Research (NCAR) and the European Centre for Medium-Range Weather Forecasts (ECMWF) by comparing the values in each dataset with measurements taken at the Russian North Pole (NP) drift stations. They also developed a gridded SAT dataset in which they used optimal interpolation (OI; Belousov et al. 1971) to combine the Russian North Pole drifting station (NP) data with data from drifting buoys and coastal land stations. Compared to the SAT measurements at the NP stations, the MM dataset was found to have higher correlations and a lower bias than the NCEP and ECMWF datasets (see Table 3, section 3). In this paper we build upon the work of MM by studying the seasonal statistics and correlations between the observations to further improve the OI analysis.

The data used in this study are 1) from drifting buoys, obtained from the International Arctic Buoy Programme (IABP); 2) NP data from the Arctic and Antarctic Research Institute in Russia; and 3) meteorological data from land stations, obtained from NCAR. These data are also combined using the objective analysis procedure, optimal interpolation, which will be discussed further in section 3d. The statistics required to estimate accurate SAT fields are the mean, variance, and measurement error of the observations and the correlation length scale (CLS) between the observations; the CLS is used to determine how much weight is given to each observation. All these quantities are estimated from the observations.

Studies of changes in SAT in the Arctic show warming trends during winter and spring (Jones et al. 1999, hereafter JNPMR; Martin et al. 1997; Chapman and Walsh 1993). As a proxy indicator of Arctic warming, Parkinson (1992) studied satellite data from the scanning multichannel microwave radiometer (SMMR) and found that the length of the sea ice season is shortening in the eastern Arctic and lengthening in the western Arctic. Thompson and Wallace (1998) show that these changes in SAT are strongly coupled to changes in sea level pressure and may be due to anthropogenic forcing of a naturally occurring mode of variability in the Arctic climate system. However, none of these studies of changes or oscillations in surface air temperature cover the entire Arctic, which has been considered a data void (Chapman and Walsh 1993). The research community has simply lacked an accurate SAT dataset, which is essential for studies of climate change. Proxies for studies of climate change such as research using satellite data have helped but have not filled this void.

In sections 2 and 3, we describe the observations, their basic statistics, and the correlations between the different types of observations. We then discuss the application of these statistics to optimal interpolation and how the seasonal statistics improve the OI analysis. In section 4, we show results from analysis of these fields.

We show the midseason monthly mean fields derived from the analysis, discuss how the analyzed fields compare to the observations, and, finally, we study spatial and temporal variations in SAT in the Arctic. Specifically, we study the interannual trends in the SAT, the length of the melt season, and the relationship of these trends to the Arctic Oscillation.

2. Data

Direct observations of air temperature over the Arctic Ocean have been collected mainly by the drifting buoys of IABP; which deployed its first buoys in 1979 (Thorndike and Colony 1980). During the early years of this program, its primary focus was on research of sea ice mechanics and wind stress on the ice. Temperatures were measured inside the buoys as a secondary variable intended mainly to be used in calibrating the barometer. Under ideal conditions, these internal temperatures can be used as a proxy for the SAT, but under Arctic conditions the use of these temperatures is fraught with problems: 1) Because of their small size (62-cm-diameter spheres), these early buoys were susceptible to being drifted over by snow; under these conditions, the buoys measured the temperature under an insulating layer of snow. 2) During summer, the temperatures within the buoys rose well above the temperature of the air due to solar heating. Since these were the primary SAT data available, the Arctic Ocean has been considered an SAT "data void" (Chapman and Walsh 1993)

In the mid-1980s the need by the research and operational communities for accurate SAT measurements was realized by the IABP, which immediately began deploying buoys with external thermistors. In 1992, the IABP began regular deployment of a new buoy design that incorporated a shielded, ventilated thermistor mounted at a height of 2 m. Tests by the IABP showed that these buoys measured SAT with an rms error of less than $0.5°C$. During any given year, 12–32 buoys reported temperatures. After 1992, four to nine of these buoys were of the new design. These data and diagrams of these buoys can be found on the IABP Web server (http://iabp.apl.washington.edu).

Recently, data from the Russian North Pole drift stations were made available by the Arctic and Antarctic Research Institute. These stations measured a myriad of meteorological quantities, including SAT in Stevenson screens at 2 m. These data are available on CD-ROM from the National Snow and Ice Data Center. This program fielded its first station in 1937; starting in 1954, one to four stations collected data from the Arctic Ocean each year. In April 1991, the last of these stations, NP-31, closed down. These observations are considered the most accurate SAT dataset for the Arctic Ocean. Finally, SAT data from more than 1600 meteorological land stations in the Arctic for the period 1979–97 were obtained from NCAR (dataset 464.0).

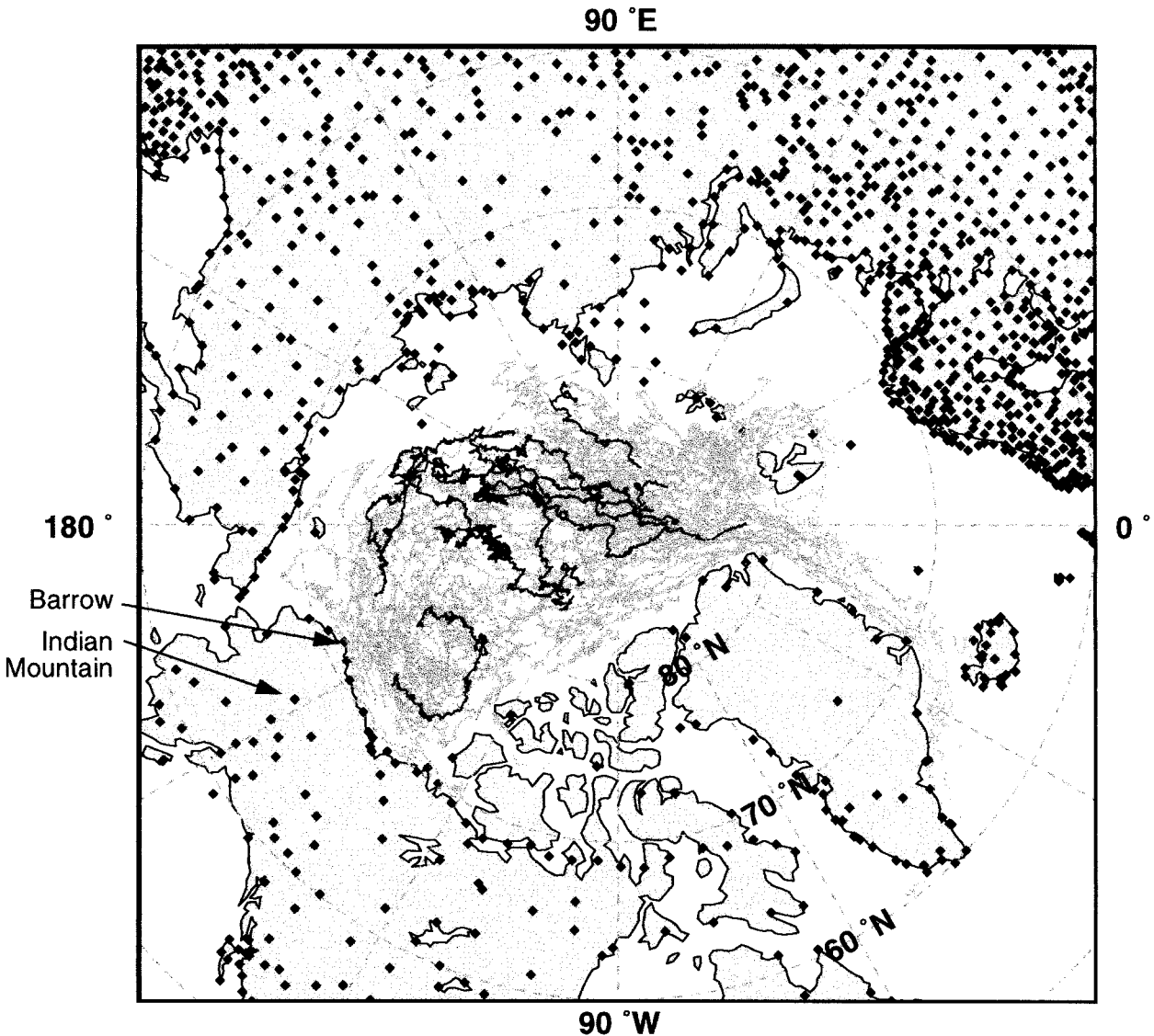Figure 1 shows the locations of the IABP, NP, and

90 °E

FIG. 1. The locations of surface air temperature observations from North Pole manned stations (black dots) from 1979 to 1991, from Argos buoys (gray dots) from 1979 to 1997, and from land stations (diamonds) from 1979 to 1997.

land observations. The buoy trajectories are shown in gray, with the trajectories of the NP stations overlaid in black. The black diamonds mark the locations of land stations. Note 1) the relatively large density of the buoy observations in the central Arctic Basin compared with the sparse NP coverage; 2) the low density of buoy observations in the Chukchi, East Siberian, and Laptev Seas; 3) the relatively large density of land stations in Europe and western Russia; and 4) the low density of coastal and interior stations in Greenland, northern Canada, Alaska, and Siberia.

All three datasets were edited to eliminate spurious data such as flyers and "flat lined" data. For the buoy data, additional checks were made for consistency with the NP data. During the isothermal summer, the buoy data were filtered to match the statistics of the NP ob-

servations; the filtering methods will be discussed later in the section on basic statistics. Questionable observations from the land stations were checked against the observations at neighboring stations. If the observations reported by any station exhibited gross errors, that is, if more than 10% of its reports were questionable during any given year, that station's data were removed from the database.

Over the Arctic Ocean we thus have accurate SAT measurements from the NP stations from 1979 to 1991. Beginning in 1992, the IABP data provides better SAT measurements from the new buoys. In section 3, we discuss the statistics of the NP observations and their use in editing the buoy data. During any given year, reliable data from 14 to 36 buoys were available for use in the OI analysis. However, since these buoys drift and

have a finite life span, during some years the spatial distribution of these observations was not sufficient to provide reliable estimates over the entire Arctic Ocean. These times and areas are flagged in the dataset.

3. Methods

a. Basic statistics

Over the ocean we used only the data from the NP stations to estimate the monthly means and variances. The land station data were divided into two groups, depending on the station's proximity to the ocean. Any land station within 50 km of the coast was considered a coastal station; all other stations were considered interior stations. The behavior of the air temperatures depends strongly on the station location. The locations of a representative coastal station (Barrow, Alaska, WMO station no. 70026) and an interior station (Indian Mountain, Alaska, WMO station no. 70174) are shown in Fig. 1. Figure 2 compares time series from each of these representative stations in 1990. Within the ocean pack ice (Fig. 2a), the SAT was close to the melt point of desalinated sea ice from late June through August. During the same period, the temperature at the Barrow coastal station (Fig. 2b) was above 0°C; however, because of its coastal environment, these temperatures are not as warm as those observed at the Indian Mountain station in the interior (Fig. 2c).

Note that an isothermal melt period can be observed in the time series for each dataset when the SAT reaches the ice melt point. During this period the SAT is maintained at about 0°C until all the snow and ice in an area have melted. For the observations at Indian Mountain, this melt period starts in March, and it is not until the end of April that SAT continues to warm above the melt point. At Barrow, this melt period begins in May and extends into June. Over the sea ice, the SAT remains close to the melt point all summer.

Figure 3 shows monthly box plots of the mean and quartiles for all the NP, coastal, and interior station data used in this study. Table 1 lists the monthly means and standard deviations of the 12-hourly observations. The isothermal summer SAT over the ocean has a mean of −0.17°C and a standard deviation (std dev) of 0.9°C. The mean July temperature at the coastal stations is 4.9°C, with an std dev of 4.5°C; for the interior stations the mean is 16.4°C, with an std dev of 5.8°C. In January, a mean of −31.4°C and an std dev of 3.6°C were found for the NP stations. Note that this std dev is an order of magnitude larger than the std dev for over-ice observations during summer. For the coastal stations the January mean is −23.5°C, and the std dev is 11.2°C; for the interior stations the mean is −16.4°C, and the std dev is 13.6°C.

b. Filtering of the buoy data

The buoy observations were edited in two ways: 1) To eliminate bad data, data with a monthly $\sigma < 0.5\sigma_{NP}$ or a monthly $\sigma > 0.5\sigma_{NP}$ were discarded (see Table 1 for σ values); 2) to adjust for summer warming of the buoys, the summer statistics of the NP stations were imposed on the buoy data.

The isothermal temperature over the Arctic Ocean provides a natural calibration point that can be easily used to correct the buoy data. A 1-week, running-mean filter was applied to impose the summer mean of −0.17°C observed at the NP stations. Any filtered buoy observation that still exceeded the maximum temperature of 1.8°C observed at an NP station was set to this value.

To illustrate, Figs. 4a–c show examples of the raw temperatures measured at three different types of buoys in 1994: an air-dropped spherical buoy (panel a), which measures SAT internally; an air-dropped Ice Experiment buoy (panel b), which measures SAT under a ventilated cap at the top of the buoy; and a new coastal environmental system (CES) buoy (panel c), which is manually installed in the ice and is equipped with a ventilated, shielded thermistor mounted 2 m above the ice surface. Unlike the temperatures measured at the NP stations, the summer temperatures measured by the buoys rise 1°–3°C above 0°C; this warming is probably due to radiational heating. Figures 4d–f show the corrected data. Note that the data from the CES buoy are almost indistinguishable from the NP observations.

c. Correlation length scales

Any observation of a geophysical quantity at one location will have a certain amount of correlation with similar observations taken nearby, where this correlation decreases with distance. The correlation length scale is an estimate of how fast this correlation decreases with distance.

The correlation between two time series is defined as the covariance between the time series normalized by the variance of each time series. The monthly box plots shown in Fig. 3 and the variances listed in Table 1 imply that the correlation between the different types of observations will vary seasonally. Although the variances of the observations are similar during winter, during summer the land station SAT variances are an order of magnitude higher than the ocean SAT variances. These variances and correlations are critical parameters in the OI analysis.

To estimate the CLS, the 12-hourly observations from each station during each month were correlated with the observations from all the other stations. That is, each interior station was correlated with all other interior stations and with each coastal, buoy, and NP station; each buoy and NP station was correlated with all other buoy and NP stations, and with each coastal and interior station, etc. These correlations were then plotted by distance. Figure 5a shows the correlations between coastal land stations and ocean stations (buoys and NP stations) during winter. The scatter of small dots shows individ-
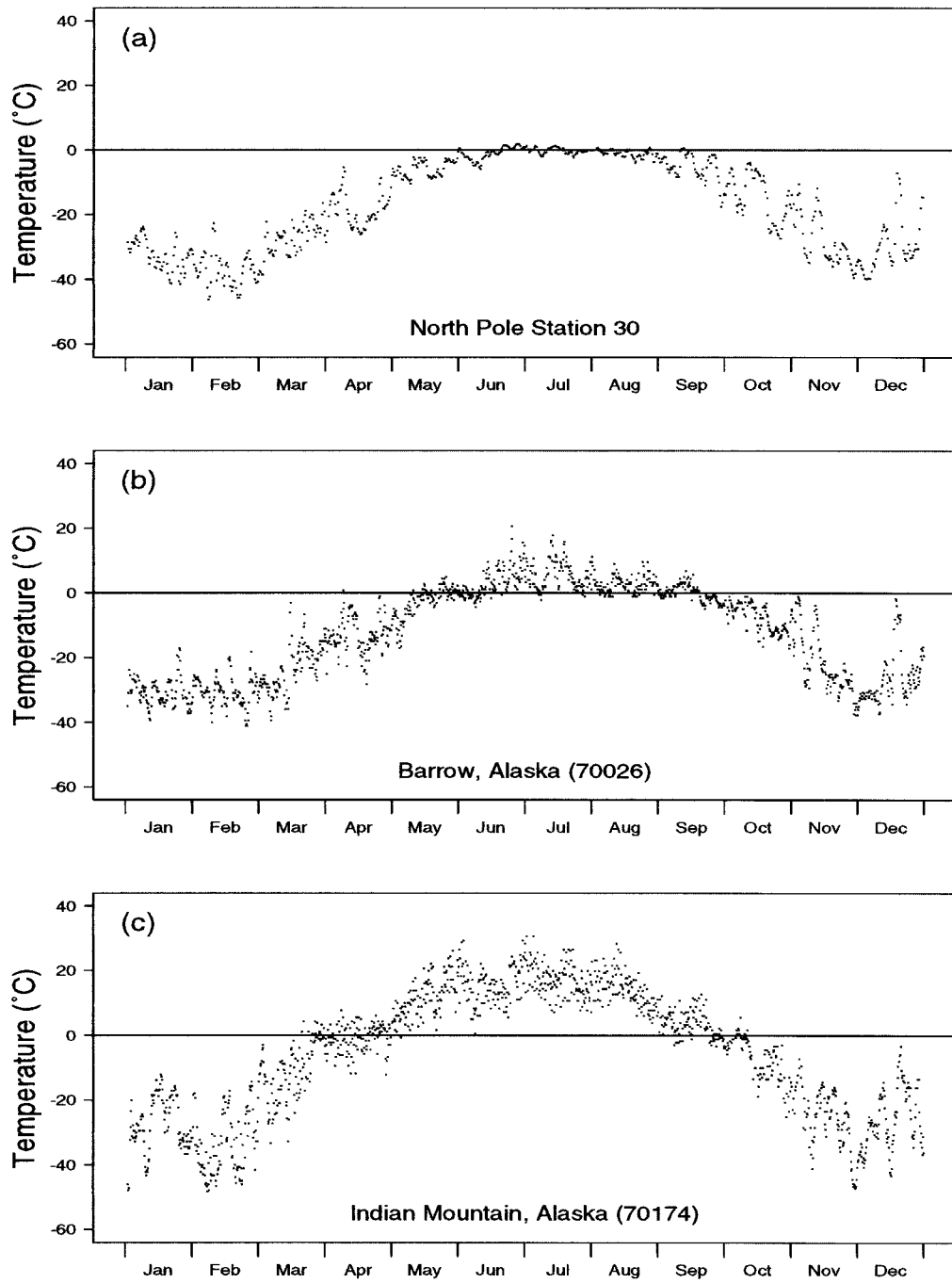
FIG. 2. Typical observations of air temperature for 1990 from a manned station on the ice (NP-30), a coastal station (Barrow, AK, WMO station no. 70026; see Fig. 1), and an interior station (Indian Mountain, AK, WMO station no. 70174). These data were collected in 1990.

ual, monthly correlations between stations. The larger dots show averages of the individual correlations separated into of 100-km bins. As the distance between pairs of stations increases, the mean of each bin decreases. The CLS is defined as the distance that the mean correlations drop below $1/e$ (Belousov et al. 1971). Figure 5a shows that the CLS between ocean observations and coastal stations is about 1000 km. Figure 5b shows the correlations between coastal land stations and ocean stations during summer. The correlations drop off much more quickly than during winter. The CLS between coastal stations and observations over ice is about 300 km.

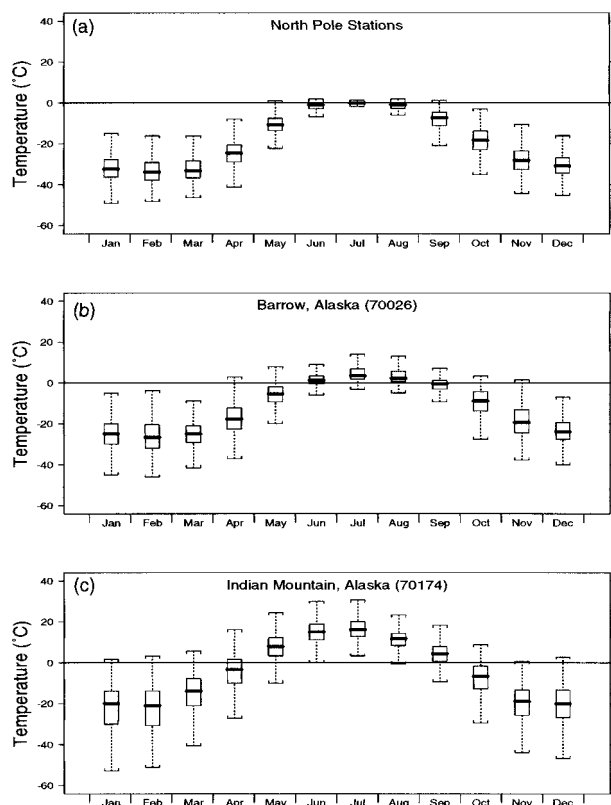To use these correlations in an OI analysis, one may

FIG. 3. Monthly box plots of 12-h air temperatures from (a) all the North Pole stations from 1979 to 1991 and from the land stations at (b) Barrow and (c) Indian Mountain from 1979 to 1997. Each box plot shows the median, and 25th and 75th percentiles; thus, half the data fall inside the box and 99% fall within the range shown by the vertical lines.

tabulate them versus distance, but in practice, an analyst may choose from a variety of functions to approximate the distance dependence of the correlations. For this study we used the function

$$R(d) = e^{-d^2/L^2}, \qquad (1)$$

where d is the distance between observations and L is the CLS. The smooth curves in Fig. 5 show this ide-

alized correlation function for the winter scale of 1000 km and summer scale of 300 km. The summer CLS between coastal and ocean data is the most difficult scale to estimate given the paucity of buoys in close proximity to the coastal stations and the inherent lack of correlation between the observations. Since the correlation function provides a good fit to the observed correlations for all other seasons and all other pairs of observations, for example, Fig. 5a, we assume the poor fit between the correlation function and the binned correlations between the coastal and ocean data during summer (Fig. 5b) is simply due to a lack of data.

Table 2 lists the correlations between different types of observations during different months. The mean CLS between the same type of observations, that is, ocean with ocean, etc., during any given month is roughly 1000 km. However, as shown in Fig. 5b, the CLSs between similar types of observations, that is, ocean with coastal, coastal with interior, are much shorter during summer. Given the short CLS for the coastal and ocean observations during summer, we assume that there is no correlation between the interior land and ocean observations.

d. Optimal interpolation

Equation (2) defines the interpolated temperature at a grid point:

$$\hat{T}_i = \overline{T}_i + \sigma_i A^T \left(\frac{Z_j - \overline{T}_j}{\sigma_j} \right), \qquad (2)$$

where $\hat{T}_i$ is the estimated air temperature at a grid point, based on the weighted deviations (A^T) of the observations Z_j from the mean $\overline{T}_i$, normalized by the variance of the observations s. In this section we discuss each component of this equation, that is, the application of the mean $\overline{T}_i$, variance s, and the weights A^T to the analysis of an OI field. Although these quantities are objective, the way they are computed may produce different results when applied in OI. For example, OI biases its estimates toward the mean chosen for use in the analysis. If 5°C were chosen, the overall mean value for

TABLE 1. Monthly statistics of 12-hourly SAT observations (°C).

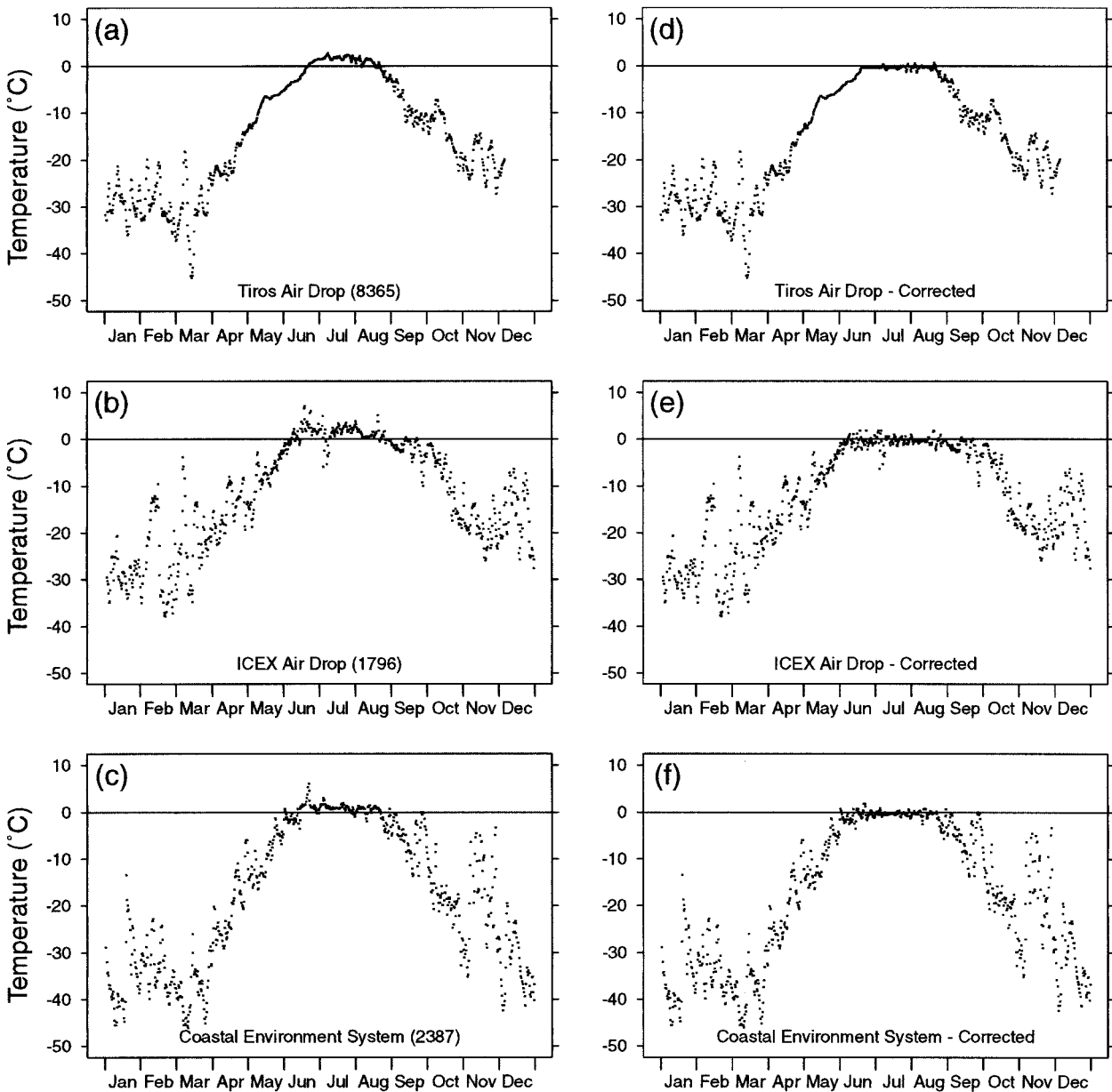|	NP mean	NP std dev	Coastal mean	Coastal std dev	Interior mean	Interior std dev
Jan	−31.99	7.27	−23.5	11.2	−16.4	13.6
Feb	−33.22	6.91	−24.2	11.6	−14.4	12.2
Mar	−32.15	6.07	−22.4	10.7	−8.0	10.4
Apr	−24.13	6.32	−16.5	9.3	−0.1	8.9
May	−10.68	4.80	−6.4	6.0	7.8	7.8
Jun	−1.88	2.31	1.3	4.2	13.8	6.6
Jul	−0.17	0.74	4.9	4.5	16.4	5.8
Aug	−1.63	1.88	3.9	4.6	14.3	6.1
Sep	−8.47	5.13	−0.2	5.1	8.5	6.1
Oct	−19.28	6.53	−8.2	8.0	0.9	8.2
Nov	−27.28	6.72	−16.7	10.2	−8.8	11.6
Dec	−30.61	6.88	−21.4	10.6	−14.2	13.2

FIG. 4. Samples of raw surface air temperature observations by different types of buoys. (a) Data from a TIROS air drop buoy, which was built by Polar Research Laboratories and has been in use by the IABP since its inception; the air temperatures reported by these buoys are internal air temperatures and not true surface air temperatures. (b) Data from an ICEX-air buoy built by Christien Michelsen Institute, Norway; these buoys measure external air temperature at the top of the buoy. (c) Data from the new "coastal environmental system" buoys built by Coastal Climate; these buoys measure a true surface air temperature at 2-m height using a ventilated thermistor. These buoys have been in use by the IABP since 1992. (d)–(f) Data corresponding to (a)–(c), respectively, corrected to match the mean statistics of the North Pole manned stations. See Figs. 2a and 3a.

SAT in the Arctic, the region as a whole would have a warm bias during winter. During summer, the land would have a cold bias, and the Arctic Ocean would have a warm bias. A careful inspection of the observations and their geophysical characteristics is imperative to produce a realistic, accurate OI analysis.

In section 3, we discussed the monthly means of the ice, coastal, and interior land station observations. Al-

though we could use these monthly values as the mean in the OI analysis, we chose to estimate a mean that varies not only seasonally but also spatially in order to capture local SAT behavior. To differentiate the mean fields used in the OI analysis from the mean fields resulting from the OI analysis, we called the means used in the analysis a monthly first guess field.

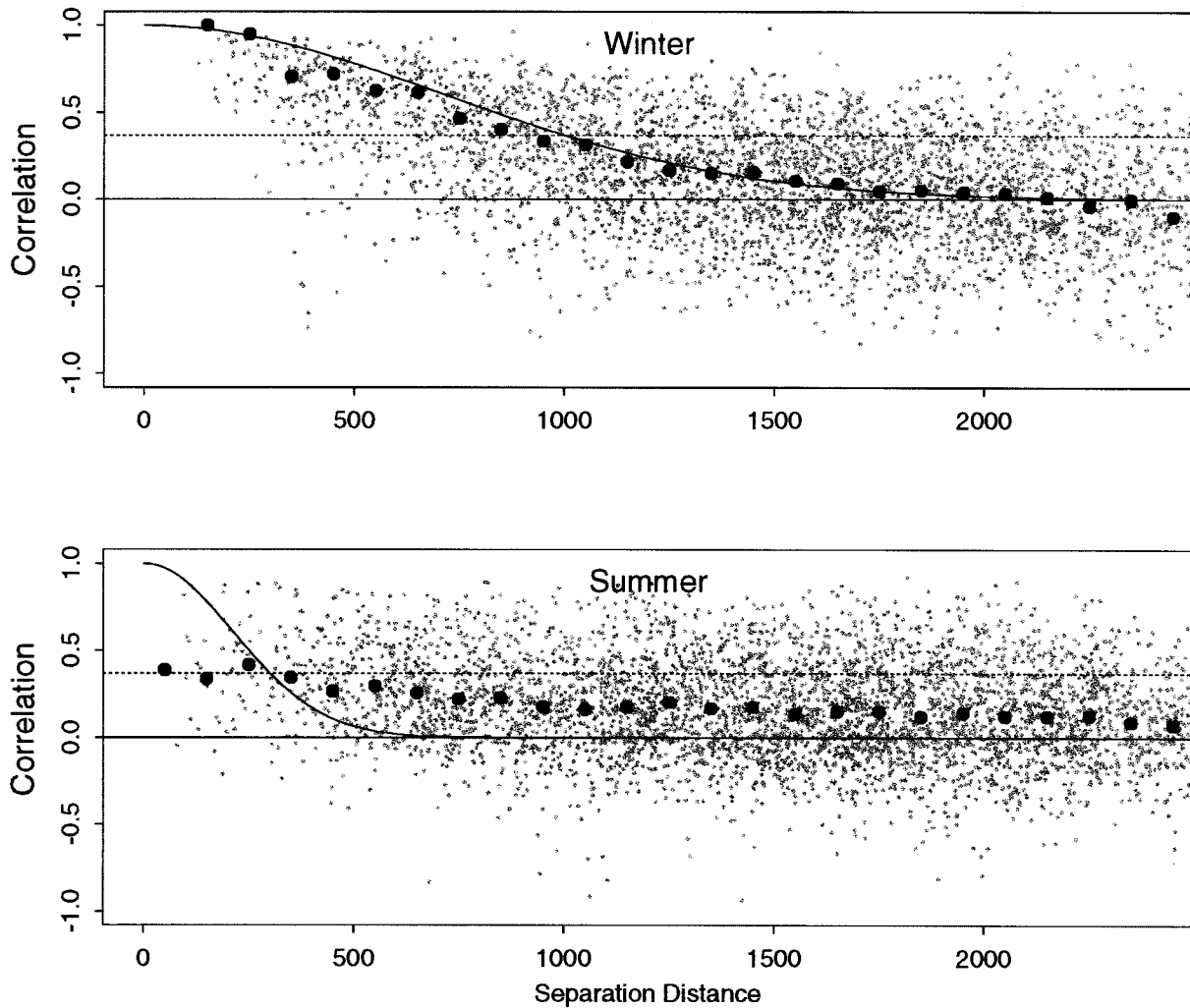To estimate the first guess fields, the observations

FIG. 5. Correlations between different pairs of coastal land stations and buoys or manned stations during (a) winter and (b) summer from 1979 to 1997. The small dots show individual monthly correlations between stations. The larger dots show averages of 100-km bins. The smooth curves show the idealized correlation function for length scales of (a) 1000 and (b) 300 km. The horizontal dashed line shows where the correlation is equal to $1/e$. (See text for explanation of smoothing function.)

TABLE 2. Monthly correlation length scales (km).

	Ocean with ocean	Ocean with coastal	Coastal with coastal	Interior with coastal	Interior with coastal
Jan	1100	900	900	900	1100
Feb	1000	1000	900	900	1100
Mar	1100	1100	900	1000	1300
Apr	1300	1300	900	1000	1300
May	1300	1300	900	900	1000
Jun	1100	500	800	800	1000
Jul	600	300	600	700	900
Aug	1000	500	600	800	1000
Sep	1100	1300	800	900	1000
Oct	1300	1100	800	1000	1200
Nov	900	1100	900	900	1200
Dec	900	1000	900	900	1100

were binned into 100-km rectangular grid boxes by month. In areas where observations were sparse, such as the North Atlantic, we chose to supplement the observations with monthly means obtained from National Centers for Environmental Prediction (NCEP) analysis (1979–96). These data were then combined in a bootstrapped OI analysis using the new CLS to produce the monthly first guess fields. Monthly variations from these first guess fields were then calculated for each type of observation for use in the OI analysis.

To get the weights A that minimize the interpolation errors, we solve the equation

$$A = \mathbf{M}^{-1}\mathbf{S},$$

where $\mathbf{M}$ is the matrix of correlations between the observations and $\mathbf{S}$ is the vector of correlations between the observations and the interpolation grid point.

A simple correlation matrix **M** with one of each of the three input types (ocean coastal, or interior) has the form

$$\mathbf{M} = \begin{bmatrix} E(T_O T_O) + \epsilon & E(T_C T_O) & E(T_I T_O) \\ E(T_O T_C) & E(T_C T_C) + \epsilon & E(T_I T_C) \\ E(T_O T_I) & E(T_C T_I) & E(T_I T_I) + \epsilon \end{bmatrix}.$$

A simple correlation vector **S**, corresponding with the above matrix **M**, has the form

$$\mathbf{S} = \begin{bmatrix} E(T_G T_O) \\ E(T_G T_C) \\ E(T_G T_I) \end{bmatrix}.$$

For **M** and **S**, the expected correlation E between observations or grid points depends on the distance between the stations or points and is given by Eq. (2); ϵ is the measurement error divided by the std dev of the data. This measurement error differs for each type of observation. Although the measurement error of the NP stations is reported to be 0.1°C, we used 0.5°C to improve the condition of the matrices. We also used 0.5°C for the new IABP CES buoys with ventilated and shielded thermistors; for all other buoys and the land stations, we used 2.0°C. In effect, the varying measurement errors in the analysis give more weight to more accurate observations.

e. Error analysis

The SATs at all grid points were analyzed using the 12 closest observations, which were also used to obtain the variance of the estimation error (in dimensionless units). In theory, all observations may be used in the analysis, but because of computational restrictions we used only 12. Thorndike and Colony (1982) found that increasing the number of inputs beyond 10 does not reduce the variance of the estimation error.

Using only a subset of the current observation, however, may introduce discontinuities in the field, since certain inputs may be used for one grid point, but other inputs may be closer for the next grid point. The magnitude of this error is assumed to be lower than the expected interpolation errors.

Figure 6 shows the analyzed fields of SAT for 16 January and 16 July 1994 as well as the variance in the estimation error for associated with each field. No confidence should be placed in variances greater than 0.5. During summer, when the CLSs between the coastal areas and the ocean are shorter, some areas of the Arctic Ocean do not have enough data to provide sufficient coverage. In these areas small discontinuities between the months may be found in the time series. However, we do not believe that this is a significant deficiency, because OI biases its estimates toward the mean. Thus in areas with insufficient coverage, the analysis will return a value close to the mean SAT. As shown in Figs.

2 and 3 and Table 1, the mean SAT over the Arctic Ocean during summer has little variance. Over land and during nonsummer seasons, for all years, there are sufficient observations to analyze accurate SAT fields.

f. Comparison of new analysis with MM and NP observations over the Arctic Ocean

To estimate the quality of their SAT analysis and that of the operational SAT datasets available from NCAR and ECMWF, MM compared each analysis with the observations from NP-28 from 1987 to 1988. For this test, the NP-28 data were not used as input into the OI analysis. Over the Arctic Ocean the MM OI SAT fields had higher correlations, lower biases, and lower rms errors than the NCEP and ECMWF fields. In a similar test, the 12-hourly estimates from our IABP/POLES (Polar Exchange at the Sea Surface) analysis were compared to NP-28 for the same period. The IABP/POLES fields had higher correlations and lower rms errors, but a higher bias, than the MM fields. It should be noted that the IABP/POLES analysis has a bias toward the 1979–97 monthly first guess fields (bootstrapped monthly mean fields). During a cold year, the IABP/POLES analysis will produce a warm bias, and vice versa during a warm year. These statistics are shown in Table 3.

The IABP/POLES analysis improves on the MM analysis in two ways: 1) The use of spatially and seasonally varying correlation length scales allows the inclusion of data from interior land stations such that a comprehensive analysis can be made over the whole of the land and ocean region in the Arctic; and 2) during summer, MM shows a warm bias of 4°–5°C in the Russian marginal seas compared to the values in the Gorschkov Atlas (Gorschkov 1983). There are two reasons for this. First, the mean used in the MM analysis is the mean of all the observations at that time. Thus in the marginal seas, where the buoy data are sparse (see Fig. 1), their OI analysis biases toward the mean of the coastal observations, which is too warm. Second, the longer CLS used by MM gives the coastal data grid points undue influence over the ocean grid points. Our IABP/POLES analysis compares more favorably with the Gorschkov atlas in the marginal seas.

As noted, a distinct difference between the MM analysis and the IABP/POLES analysis is the choice of means. Although MM's choice of using the mean of all observations provides a lower bias in the central Arctic, this choice introduces a large bias over the marginal seas. This choice produces a warm bias in colder years, and vice versa. As shown in the comparison to NP-28, this bias is about ±0.5°C.

g. Reanalysis products from NCEP and ECMWF

The NCEP (i.e., NCAR) and ECMWF datasets have recently been reanalyzed, but our examination of these datasets show that they still need work. The NCEP

Analyzed field for January 16,1994   Error variance field for January 16,1994

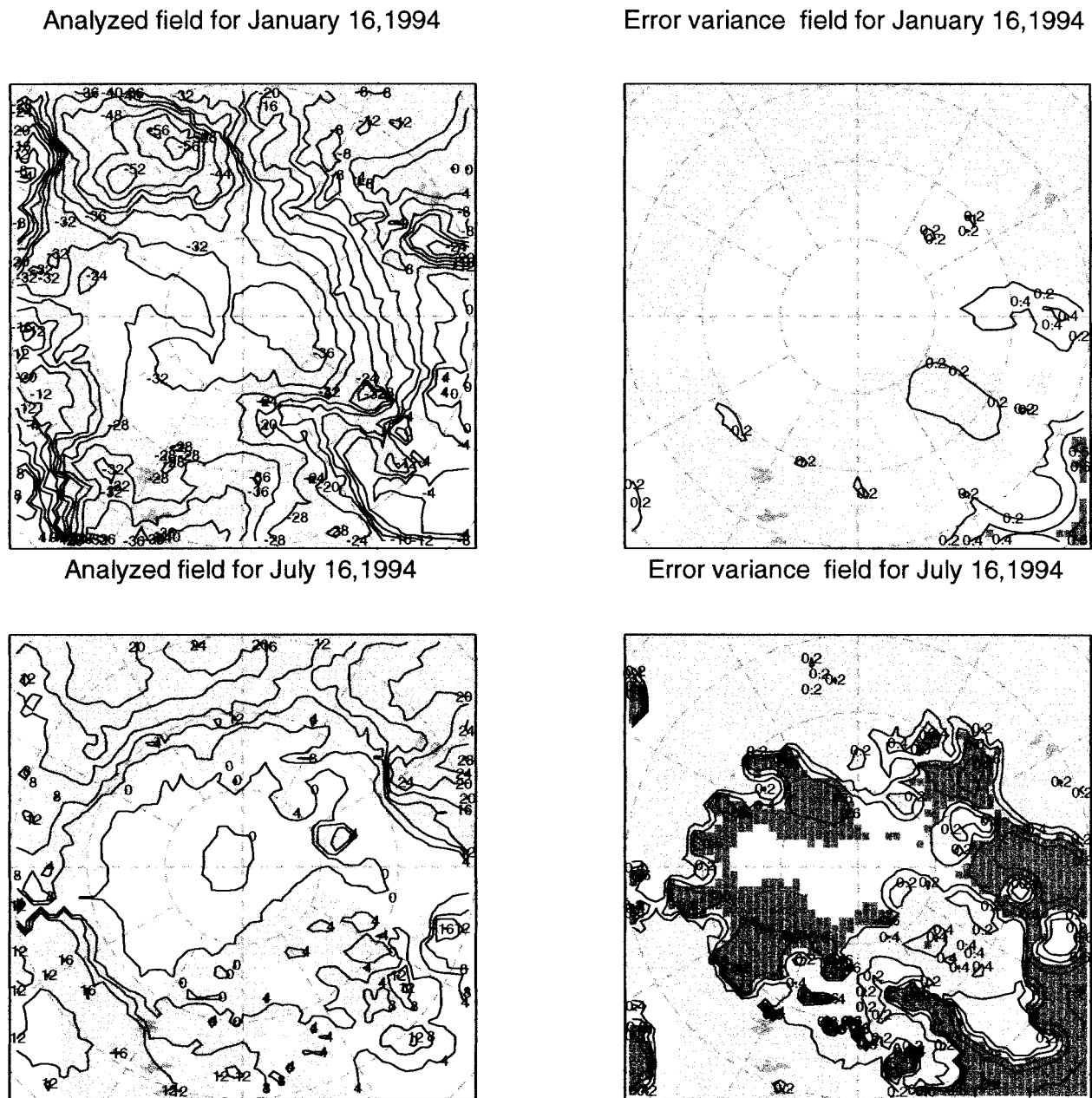Analyzed field for July 16,1994   Error variance field for July 16,1994

FIG. 6. Analyzed SAT fields for (top left) 16 Jan 1994 and (bottom left) 16 Jul 1994. The variance fields of the estimated errors (unitless) for each day are shown to the right. Black boxes at lower right mark areas with insufficient coverage.

fields, for example, suffer from an artifact of the analysis procedure called spectral ringing, which introduces unrealistic periodic patterns in SATs at the poles, and the ECMWF fields show a summer mean temperature of $-1.8°C$, that is, the freezing temperature of seawater rather than the melt temperature of desalinated sea ice as observed at the NP stations.

4. Results

Twelve-hourly SAT fields have been analyzed from 1979 to 1997. Figure 7 shows the midseason monthly mean fields derived from this analysis. These and the other monthly mean SAT fields can be obtained from the IABP Web server. Over the entire Arctic region, January is the coldest month, while July is the warmest. Over the ocean, the coldest region is north of the Canadian archipelago, and during summer the SAT over the ocean is held to an isothermal value of $-0.2°C$.

Caution should be taken in using IABP/POLES SAT data for the North Atlantic and over Greenland since the analysis uses only buoy and NP data collected over the Arctic Ocean and there are few observations from

TABLE 3. Comparison of NP-28 SAT observations with the SAT values in four datasets from the period Jan 1987–Dec 1988. A positive bias means the dataset is warmer than the observations.

Dataset	Correlation	Bias	Rms error
Entire period			
IABP/POLES	0.82	0.5	2.5
POLES*	0.77	0.2	3.2
NCEP*	0.78	0.5	3.2
ECMWF*	0.37	1.1	5.2
Summer (Jun–Aug)			
IABP/POLES	0.62	0.4	1.1
POLES*	0.66	0.0	1.3
NCEP*	0.42	1.3	1.3
ECMWF*	0.44	−0.4	2.1
Winter (Nov–Mar)			
IABP/POLES	0.84	0.1	2.83
POLES*	0.80	0.1	3.7
NCEP*	0.83	0.2	3.0
ECMWF*	0.27	2.2	6.1

* From Martin and Munoz (1997).

the interior of Greenland (see Fig. 1). The results for the interior of Greenland have therefore been excluded from the following studies of variation, and the results for the North Atlantic should be regarded with caution.

a. Trends

Trends in Arctic SAT have been studied by Chapman and Walsh (1993) using the East Anglian SAT dataset from 1961 to 1990 (Jones et al. 1986) and by Martin et al. (1997) using SAT measurements from the NP stations from 1954 to 1991. Following the methods of Chapman and Walsh (1993), JNPMR studied trends through 1998. All these studies find warming trends in the Arctic during winter and spring. Although Chapman and Walsh (1993) and JNPMR show the spatial patterns of this warming over land, Martin et al.'s (1997) study shows only temporal trends in SAT over the ocean. Using the IABP/POLES dataset, we redo these analyses to study the spatial nature of the trends over the entire Arctic Ocean extending south to 60°N.

Trends were evaluated by least squares fits of the annual and season temperatures for each grid cell. The seasons were defined as December–February (winter), March–May (spring), June–August (summer), and September–November (autumn). The significance of each trend was calculated using a Student's t-test for accepting the hypothesis that there is no trend. Figures 8 and 9 show the annual and seasonal trends north of 60°N. Trends in grid cells that are significant at the 95% level are marked with small white dots; trends that are significant at the 99% level are marked with small black dots. Note that over the whole domain, most of the interannual and seasonal trends, except spring, are insignificant. Note also the spatial variability and the coherence between all seasons except summer.

Compared to Chapman and Walsh (1993), some sim-

ilar patterns can be found: 1) warming dominates during winter and spring, 2) the areally averaged trend for the summer is nearly zero, and 3) there is significant warming over northern Eurasian land areas. This warming is shown in this analysis to extend out over the eastern Arctic Ocean.

Some differences compared to Chapman and Walsh (1993) are 1) there is a cooling trend in the Canadian Beaufort Sea during autumn and winter, 2) the warming trend in Alaska and northwest Canada has weakened, and there is even a cooling trend in northwest Canada during fall, and 3) a warming trend is shown in eastern Greenland, Iceland, the North Atlantic, Europe, and Eurasia during winter.

JNPMR review changes in SAT during the past 150 years, 1850–1998. In their work, they use the methods of Chapman and Walsh (1993) to study trends during two 20-yr periods of significant warming: 1925–44 and 1978–97. Their results for 1978–97 show patterns over land similar to those shown in Figs. 8 and 9. We assume that the differences between these two new studies and Chapman and Walsh's (1993) work are due to differences in the periods studied.

Over the Arctic Ocean, the annual trends show a warming of about 1.0°C (decade)$^{-1}$ in the eastern Arctic, primarily in the area north of the Laptev and East Siberian Seas, whereas the western Arctic shows no trend, or even a slight cooling in a small portion of the Canadian Beaufort Sea.

During fall, the trends show a significant warming of 2°C (decade)$^{-1}$ over the coasts of Greenland, near Iceland, and in Siberia but a cooling of 1°C (decade)$^{-1}$ over the Beaufort Sea and Alaska. During winter, the trends show a significant warming of up to 2°C (decade)$^{-1}$ in eastern Greenland and Europe and 2°C (decade)$^{-1}$ over Eurasia, extending north over the Laptev Sea; however, a cooling trend of 2°C (decade)$^{-1}$ is shown over the Beaufort Sea and eastern Siberia extending into Alaska. The cooling trend over eastern Siberia is significant. During spring, a significant warming trend of 2°C (decade)$^{-1}$ can be seen over most of the Arctic. Summer shows no significant trend.

These results agree with the changes noted in sea ice concentration observed from satellite data. Using SMMR data, for example, Parkinson (1992) notes a shortening of the sea ice season in the Eastern Hemisphere and a lengthening in the Western Hemisphere. Maslanik et al. (1996) show that the reductions in sea ice cover in the Siberian sector of the Arctic Ocean continue through 1993. They attribute these changes to the increase in cyclone activity over the central Arctic Ocean and note that since 1989 there has been a sharp increase in cyclone activity north of Siberia. In Fig. 4 of their paper, they show the spatial distribution of changes in cyclone activity from 1982 to 1993. During this 12-yr period, there was an increase in the number of cyclones over the eastern Arctic and a decrease in the western Arctic. The location of the cyclonic anomaly

favors stronger and more frequent warm, southerly advection in the east Arctic. They also show an increase in anticyclones in the west Arctic. This anomaly favors cold, northerly advection in the west Arctic. These changes in sea ice coverage, cyclone activity, and SAT trends also coincide with the decrease in sea level pressure (SLP) and the enhanced cyclonic regime noted by Walsh et al. (1996), which continues through the present.

b. Onset of melt and freeze and the length of the melt season

The ice and snow masses in the polar regions interact with the global climate system in a myriad of complex ways. During most seasons, SAT trends can be studied by simple statistical methods, but during summer, because these masses hold the SAT to the melting point of sea ice, detection of changes in SAT must rely on other, less direct indicators such as the length of the melt season. The melt season is defined as that period when the SAT is near or above the melting point of ice.

Detection of the onset of melt and freeze from SAT data obtained at the NP stations was studied to some extent by Colony et al. (1992). They suggest a number of ways to estimate the onset of melt and freeze from SAT observations. One is to apply a least squares fit to the warming and cooling periods and then define melt as the intersection of the resulting lines with 0°C. This method requires a number of assumptions, such as the time span of the warming and cooling periods. Alternatively, they suggest using a 2-week running median filter and defining the onset of melt and freeze as the day that the filtered data rise or drop below the melting temperature of sea ice. The only assumption required by this latter method is the definition of the melting temperature of sea ice. Martin and Munoz (1997) chose −0.1°C, and Colony et al. (1992) and Lindsay (1998) chose −0.5°C; Andreas and Ackley (1982) suggest that the sea ice begins to melt when the SAT rises above −1.9°C, the threshold temperature for conduction of heat from the ocean up through the ice. We chose an intermediate value of −1.0°C. As shown by Colony et al. (1992) and in Fig. 9, this range of choices for the melt point would, at most, change the onset of melt and freeze by about a day.

In their study of the onset of melt and freeze based on the NP data, Colony et al. (1992), found that the onset of melt occurred at most stations between 15 and 19 June. The earliest was 11 June, and all stations were at the melt point by 30 June. For most stations the onset of freeze occurred between 12 and 22 August, so that the duration of the melt season was about 60 days.

To estimate the onset of melt and freeze from the IABP/POLES SAT analysis, we first computed daily averages of the 12-hourly fields from 1979 to 1997 and then applied a 2-week running mean filter with a threshold of −1.0°C to the time series of each grid point. Figures 10 and 11 show the mean onsets of melt and

freeze derived from this analysis. On average, melt begins over Siberia, Alaska, northern Canada, and the North Atlantic on the first of May. By the first of June, melt has advanced to the edge of the marginal seas, into the Canadian archipelago, and into the Greenland and Barents Seas. The advance of the melt isotherm stalls at the coast and margin of the Arctic Ocean for a few weeks, slowed by the large mass of snow and ice over the ocean. This stall also occurs in the observations shown in Fig. 2. Once the entire mass of ice is brought near to the melt point, melt then advances rapidly over the Arctic Ocean, reaching the pole on 19 June, 2 weeks later. The last area to reach the melt point is the Lincoln Sea, adjacent to northern Greenland, which begins to melt on 21 June, 2 days after the pole.

Figure 11 shows that the onset of freeze occurs at the pole on 16 August, and the freeze isotherm advances more slowly than the melt isotherm. Freeze returns to the marginal seas a month later than at the pole, on 21 September. Figure 12 shows the length of the Arctic melt season. Near the North Pole, the length of the melt season is about 58 days, while in the marginal seas, the melt season is about 100 days. The dates for the central Arctic compare exactly to the dates of onset of melt and freeze found by Colony et al. (1992) from NP data. Figure 11 also shows the lag in the freeze onset over the marginal seas as observed by MM, which is caused by the heat retention in open water adjacent to the coast.

The onset of melt and freeze of Arctic ice pack can be detected in satellite data by the abrupt change in backscatter when the sea ice begins melt. Although satellites do not provide coverage over the entire Arctic Ocean, the data can be used to check our analysis in areas of coincident coverage. For 1992, Winebrenner et al. (1994) showed that the onset of melt and freeze could be observed from European Remote Sensing Satellite (ERS-1) Synthetic Aperture Radar data. He found that melt in the Beaufort Sea began on 13 June at 73°N and advanced to 83°N by 20 June. If we assume that the advance of melt follows this pace from the marginal seas to the pole, the melt isotherm should reach the pole in 2 weeks. Using visible-band satellite imagery, Robinson et al. (1992) studied the variability of snowmelt in the Arctic Basin from 1975 to 1988. They found that snowmelt begins in the Beaufort and Chukchi Seas by the end of May, melt begins in the Laptev and East Siberian Seas on June 14, and melt advances to the central Arctic by 23 June (Table 1 of Robinson et al. 1992). Assuming that once melt starts over the central Arctic, it advances rapidly to the pole; comparison of these results with Fig. 10 shows that our results agree almost exactly in the marginal seas, but we find that onset of melt at the pole is earlier by 4 days. Using microwave data from 1979 to 1986 covering an area from roughly 73° to 84°N (primarily in the Beaufort Sea), Smith (1998) shows that the onset of melt also occurs on 13 June and the onset of freeze on 28 August, for a mean melt season of 75 days. Our analysis
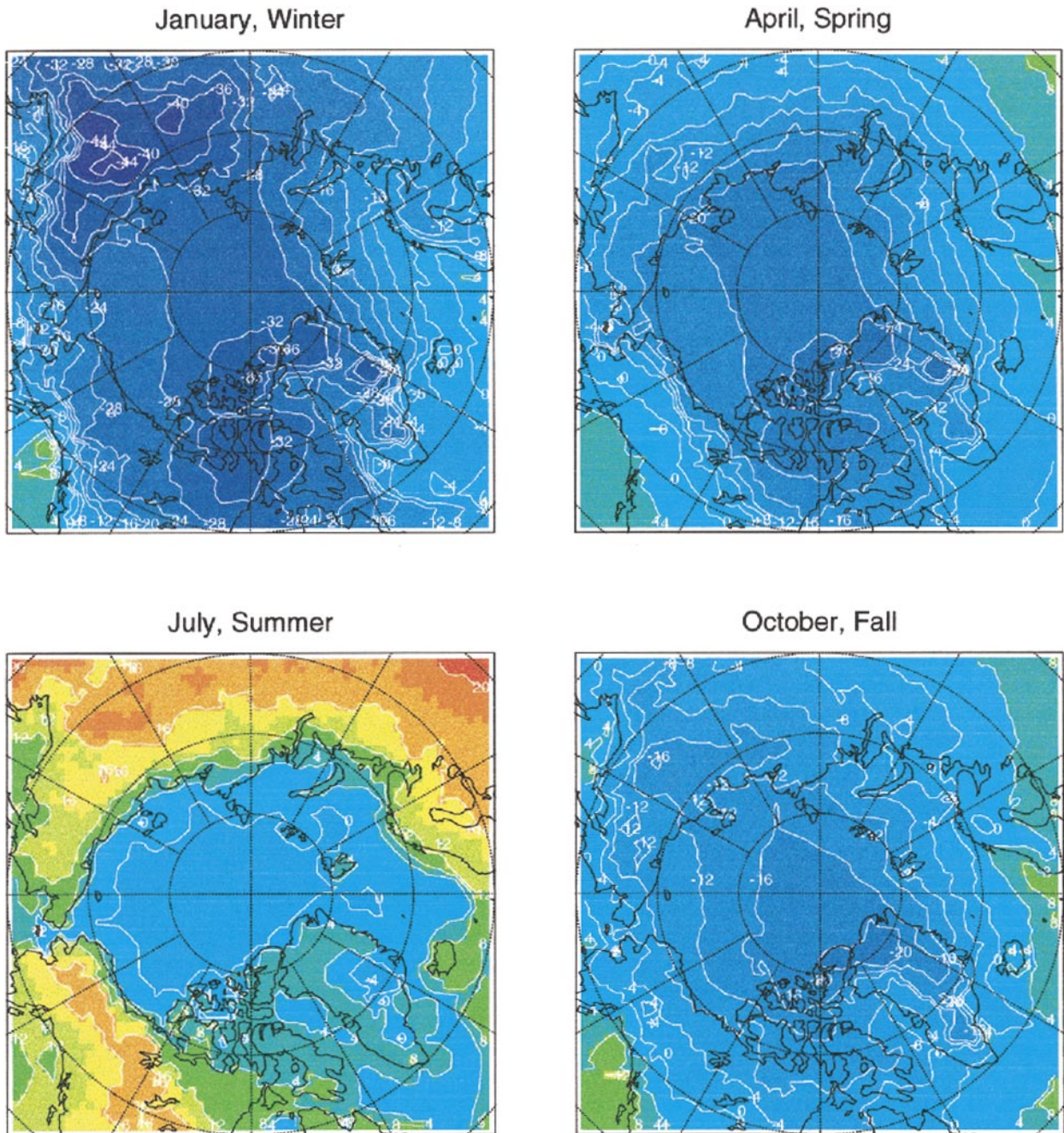
January, Winter

April, Spring

July, Summer

October, Fall

FIG. 7. Midseason mean fields of surface air temperature (°C) calculated from optimally analyzed fields from 1979 to 1997.

shows a mean melt season for the same area of about 70 days.

Compared to the MM estimates of the onsets of melt and freeze, the IABP/POLES analysis shows a much faster advance of the melt and freeze isotherms. Although MM's onsets of melt and freeze are comparable to those of the IABP/POLES analysis and the satellite data for the marginal seas, we believe that their the slower advance of the melt and freeze isotherms over the central Arctic Basin is due to their choice of a melt threshold of −0.1°C, since

the mean isothermal, summer SAT over Arctic sea ice is −0.17°C, and their data were filtered through a running median filter. At the coast this arbitrary choice is not detrimental since the SAT rises well above the melt temperature, but over the sea ice, the chance of the median value of SAT rising above −0.1°C is low. Martin and Munoz (1997) estimate that the length of the melt season in the central Arctic is about 1 month, that is, the month of July, compared to the 60 days found by this study and Colony et al. (1992) for the NP data.
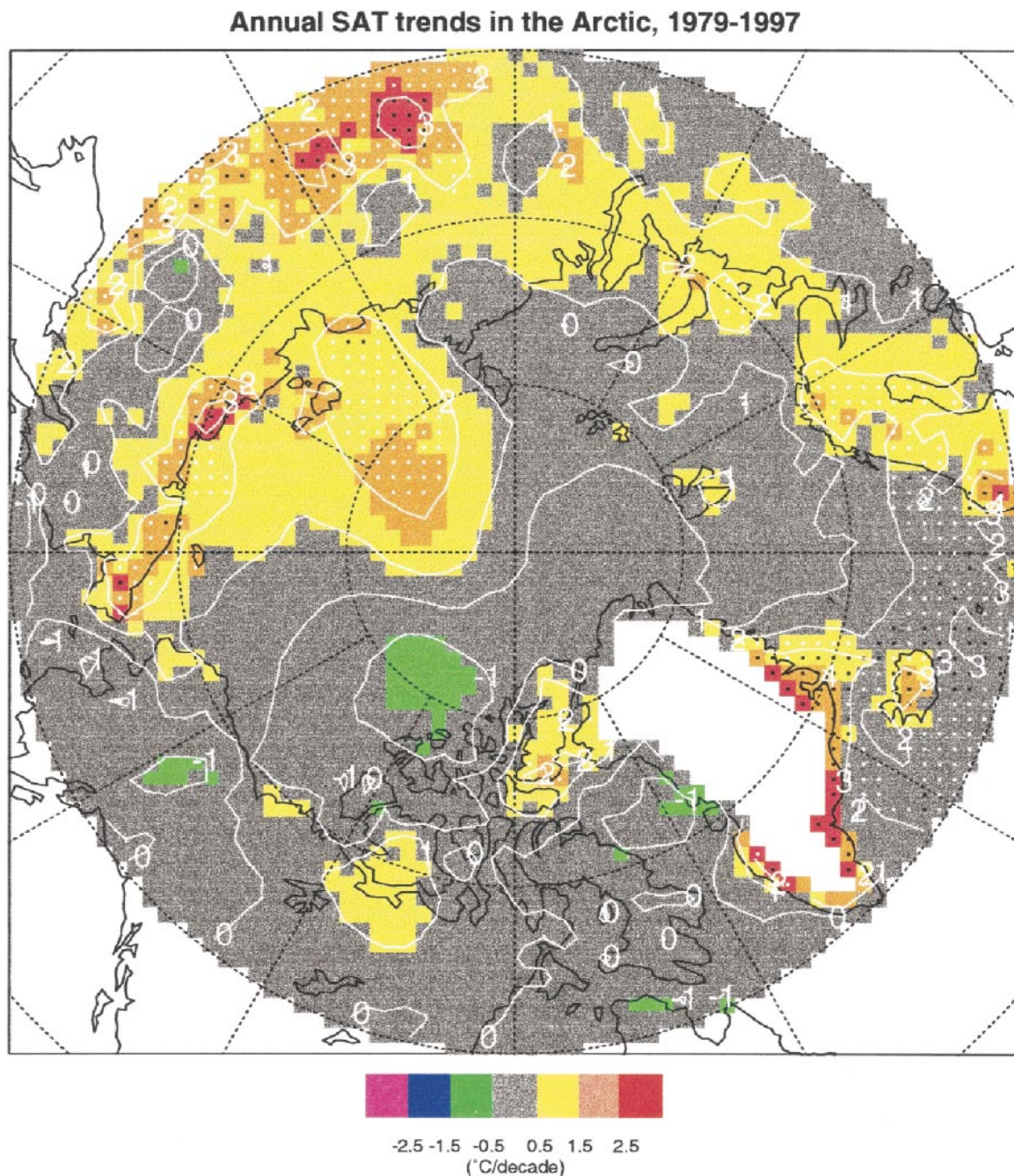
Annual SAT trends in the Arctic, 1979-1997

FIG. 8. Annual trends in SAT from IABP/POLES dataset for 1979–97.

Figure 13 shows areal averages of the onset of melt and freeze and the length of the melt season. These trends show a lengthening of the melt season in the eastern Arctic of 2.6 days (decade)$^{-1}$ due to an earlier onset of melt and a later onset of freeze, and a shortening of the melt season in the western Arctic of 0.4 days (decade)$^{-1}$, primarily due to earlier autumn cooling. Note that these trends are insignificant.

Using SMMR and Special Sensor Microwave/Imager

satellite data from 1979 to 1996, Smith (1998) did a similar study of the melt season in the Arctic. He found a significant increasing trend of 5.3 days (decade)$^{-1}$ in the length of the melt season. Since the predominant area for which he was able to estimate melt and freeze was in the Beaufort Sea (73°–84°N and 170°–270°E), his results disagree with ours. For the same area we find a decreasing although insignificant trend (see Fig. 13). Although the patterns of the onsets of melt given by

Winter (DJF)

Spring (MAM)

Summer (JJA)

Fall (SON)

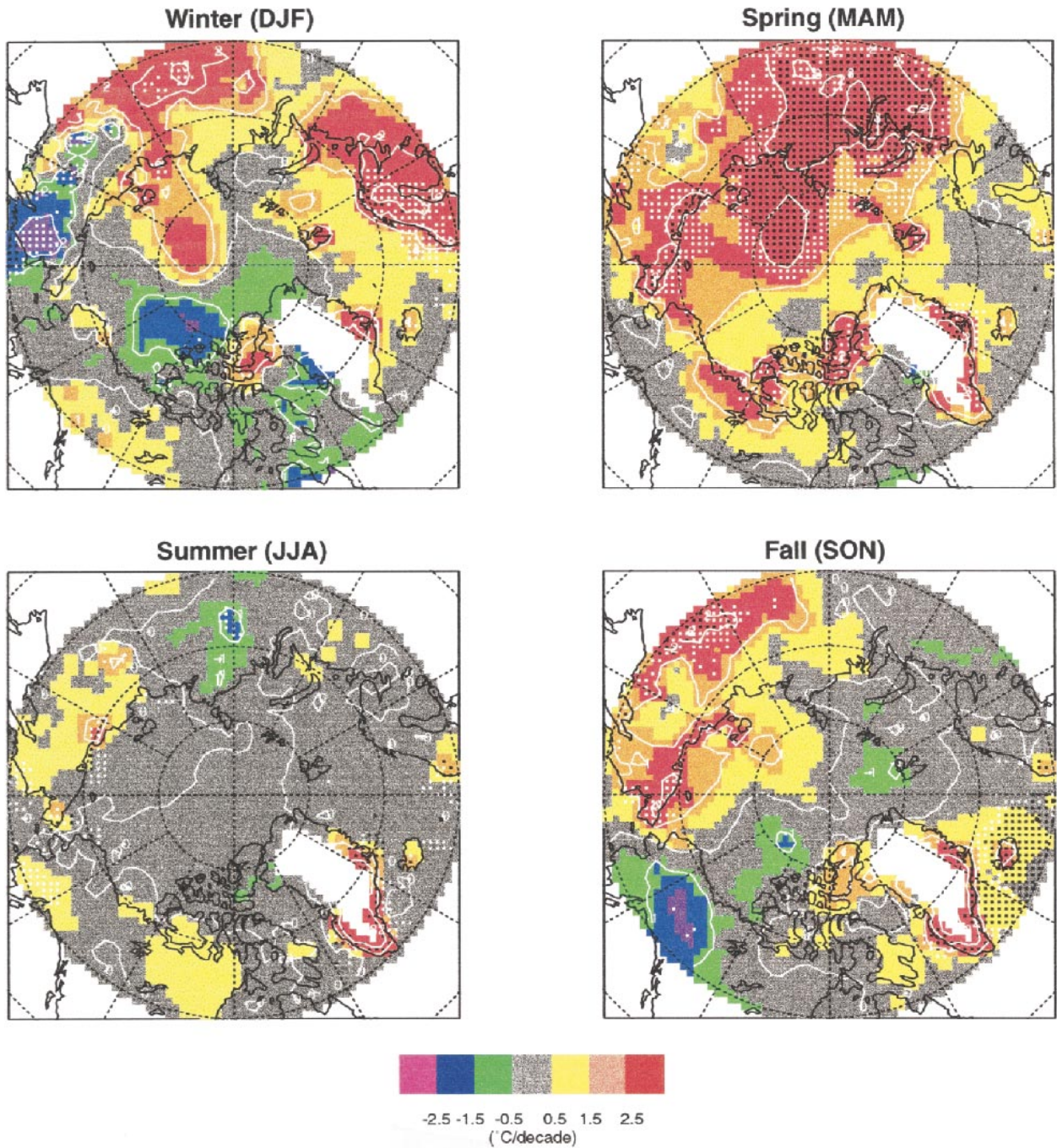-2.5 -1.5 -0.5 0.5 1.5 2.5
(°C/decade)

FIG. 9. Seasonal trends in SAT from IABP/POLES dataset for 1979–97.

both studies agree, the onsets of freeze (from which Smith gets most of his trend) show no correlation. When using satellite data, the onset of melt produces a distinct jump in the brightness temperature measured by the satellite. However, since the freezing process must overcome all the latent heat stored in brine pockets and melt ponds, false drops can occur in the brightness temperature that make detection of the onset of freeze more difficult. Given that there are no systematic differences

in the detection of melt and freeze when using the direct method proposed by Colony et al. (1992), as there are in the complicated algorithms used for satellite data, we believe that the straightforward method provides a more robust estimate of the length of the melt season. Also, in contrast to Smith's (1998) results and using the same dataset, Parkinson (1992) finds a lengthening of the sea ice season in the western Arctic, which agrees with our results.
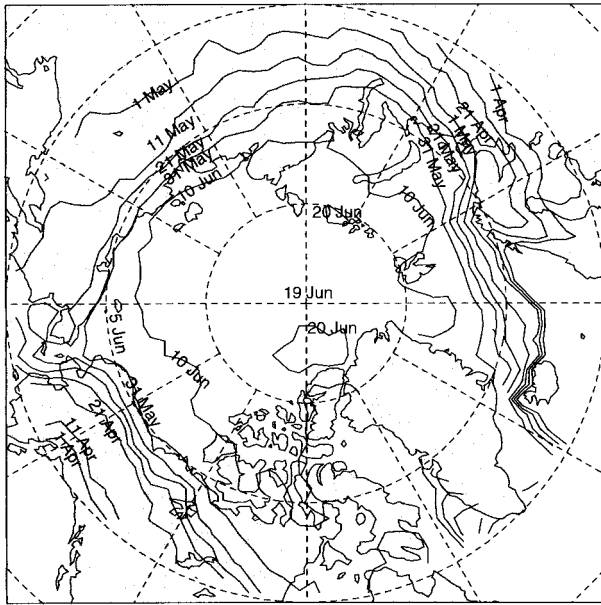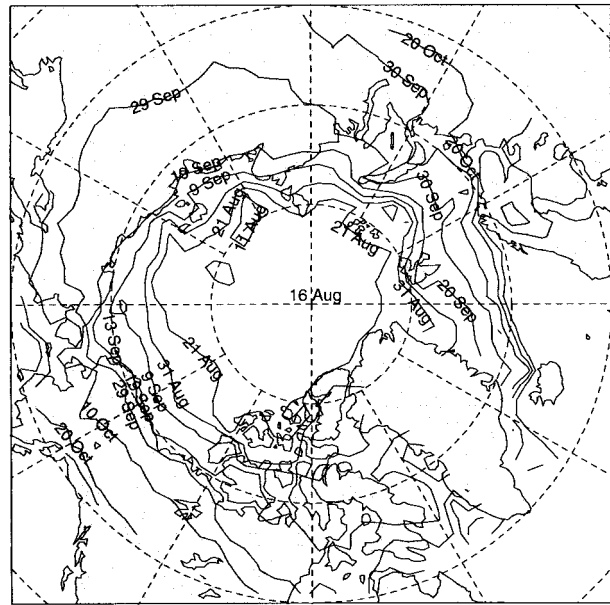
FIG. 10. Onset of melt.

FIG. 11. Onset of freeze.

c. The Arctic oscillation

The Arctic oscillation (AO; Thompson and Wallace 1998) is the first principal component of the empirical orthogonal function of SLP in the Northern Hemisphere. This is a robust pattern that dominates the SLP record and can be interpreted as the surface signature of modulation in the strength of the polar vortex aloft (Thompson and Wallace 1998). Using the East Anglian SAT dataset, Thompson and Wallace (1998) show that the AO accounts for more than half of the winter (November–April) warming over the Eurasia land areas. Following Thompson and Wallace's (1998) analysis of SAT trends over the northern land areas, we estimate the contribution of the AO to trends in SAT over the Arctic Ocean. Figure 14a shows the SAT trends in winter (December–February), and Fig. 14b shows the contribution of the AO to the SAT trends. The contribution of the AO is estimated by regressing the SAT on the AO index and then multiplying by the trend in the AO (1.186 std devs (decade)$^{-1}$ from 1979 to 1997). It should be noted that the regression may also produce a negative relationship, but for which the AO may still explain a significant portion of the variance in the SAT trend. As such, we take the absolute value of the regression. The residual SAT trends not explained by AO-related contributions are shown in Fig. 14c, and the fraction of the SAT trend explained by the AO is shown in Fig. 14d. The areas where the AO explains more than 50% of the SAT trend are shown in yellow, and the areas where the AO explains less than 50% of the SAT trend are shown in gray. Over the Arctic Ocean, the AO evidently accounts for 74% of the warming over the eastern Arctic Ocean and 14% of the cooling over the western Arctic

during winter, but the AO does not explain the trends over eastern Siberia nor over the Canadian archipelago.

5. Conclusions

Using the monthly statistics and the new correlation length scales, we improve on MM's OI SAT analysis in several ways. First, we are able to include data from interior land stations and extend the analysis over land without any undue side effects over the ocean. Second, the temperatures in the Russian marginal seas during
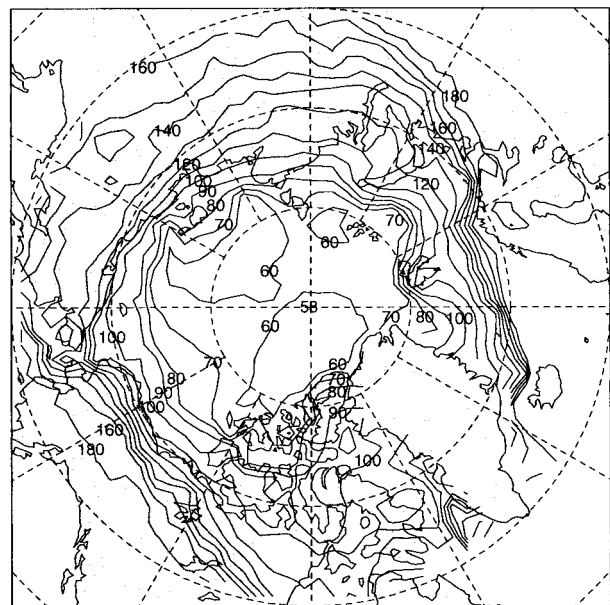

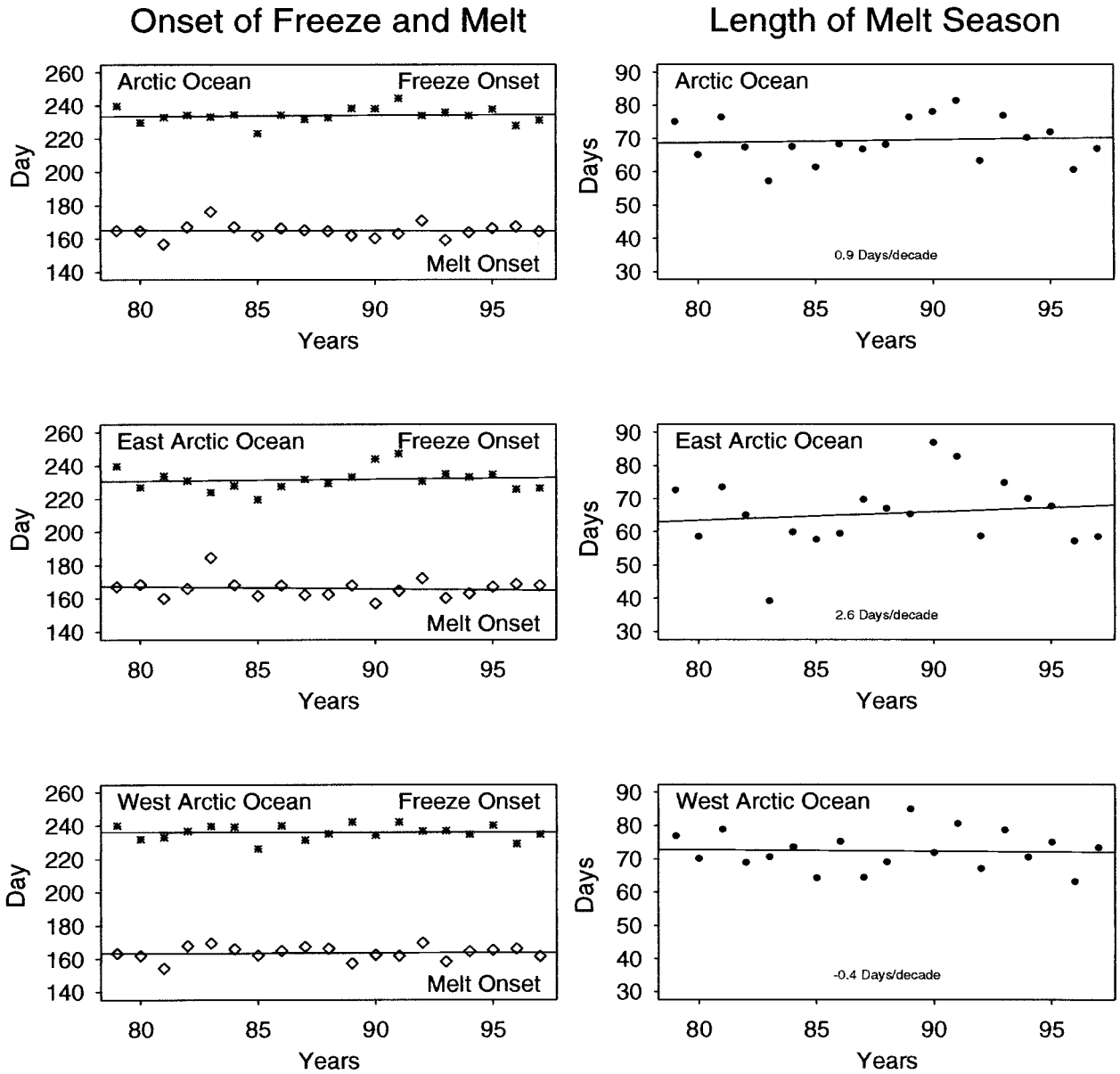FIG. 12. Length of the melt season (days).

FIG. 13. Areal trends in the length of the melt season. Column (a) shows the onset of melt and freeze and the length of the melt season over the entire Arctic Ocean. Column (b) shows the same for the eastern Arctic Ocean, and (c) for the western Arctic Ocean.

summer have more realistic means of 1°–2°C with std devs of 1°C versus the means of 2°–4°C with std devs of 4°C estimated by MM, which are more characteristic of the coastal station data than observations over the ocean. Third, the onsets of melt and freeze and the length of the melt season derived from our analysis match the observations at the NP stations and the satellite observations much more closely.

The CLSs between SAT observations depend on the location and season. The CLSs between homogeneous pairs of stations are about 1000 km. The CLSs between mixed types of stations are shorter, about 900 km, and even shorter during summer when the CLS between

observations over the ice and at the coastal land stations drops to 300 km. We believe that the summer CLS between the ocean observations and the interior land observations is negligible.

The period 1979–97 is one of the greatest warming periods during the past 150 yr in the global climate record and is the warmest period on record (Jones et al. 1998). Over the globe, JNPMR found this warming to be 0.16°C (decade)$^{-1}$ and that this warming was greatest during winter and spring.

Over the Arctic land areas, warming trends in the SAT of 1°C (decade)$^{-1}$ and 2°C (decade)$^{-1}$ (1978–87) were found by Jones et al. and by this study (1979–97)
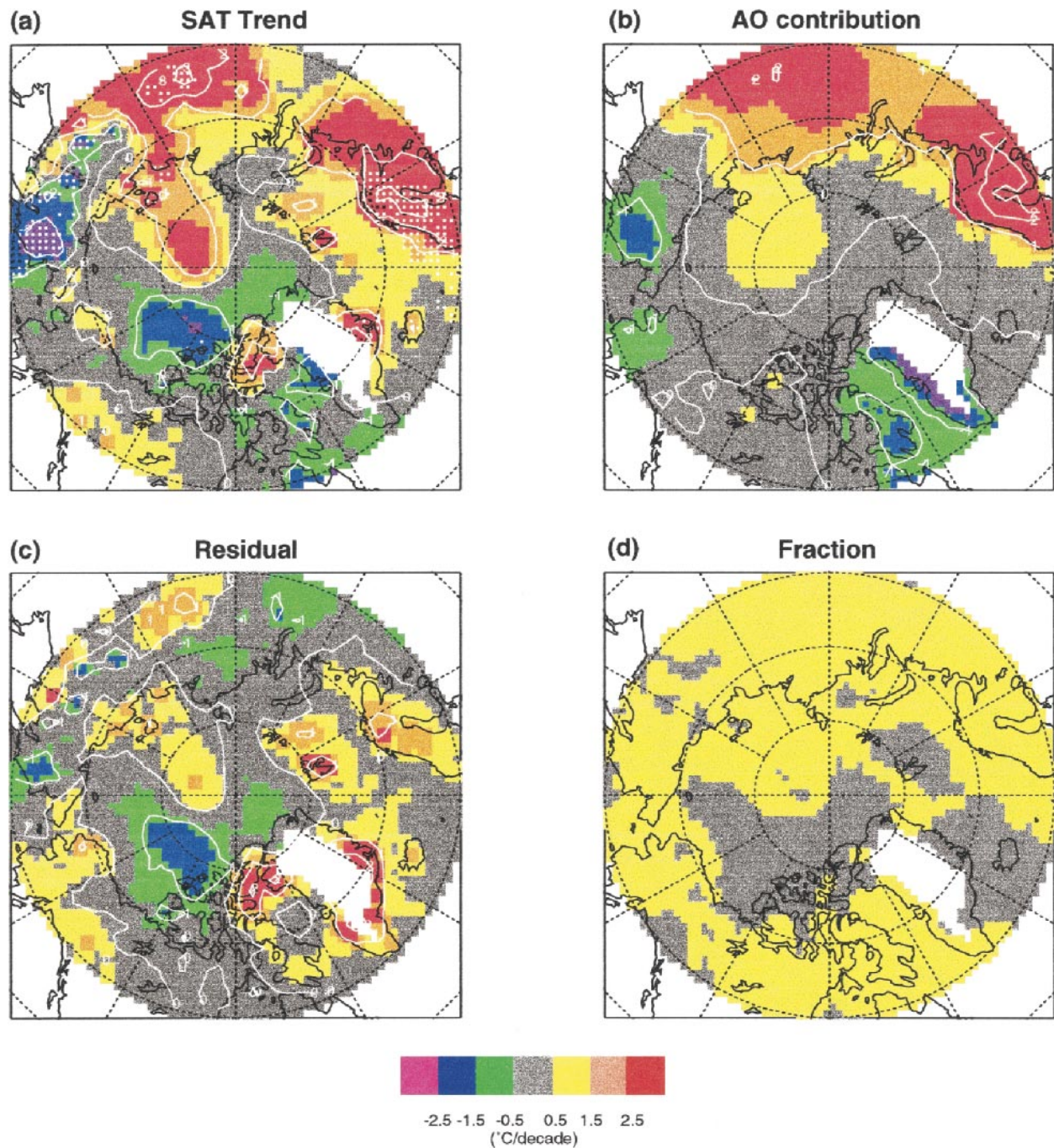
FIG. 14. Contribution of the Arctic oscillation to winter (Dec–Feb) SAT trend. (a) SAT trend; (b) AO contribution to SAT trend; (c) residual SAT trends not explained by AO; (d) fraction of SAT explained by AO. The areas in Fig. 4d where the AO explains more than 50% of the SAT trend are shown in yellow, and the areas where the AO explains less than 50% of the SAT trend are shown in gray.

during winter and spring, respectively. A cooling trend of 2°C (decade)⁻¹ was also found over eastern Siberia. This trend is significant at the 95% level. The warming trend during spring spans most of the Arctic region and is significant at the 95% level over most of the eastern Arctic.

The winter and spring warming over the Eastern Hemisphere landmasses extends out over the eastern Arctic Ocean, where the trends are 1°C (decade)⁻¹ and 2°C (decade)⁻¹, respectively. The spring warming trend over the eastern Arctic Ocean is significant at the 99% level. The western Arctic Ocean and Alaska show no trend or even a cooling trend of 1°C (decade)⁻¹ during winter.

On average, we find that melt begins in the marginal seas by the first week of June and advances rapidly over the Arctic Ocean to reach the pole by 19 June, 2 weeks later. The onset of freeze occurs at the pole on 16 August, and the freeze isotherm advances more slowly than the melt isotherm. Freeze returns to the marginal seas a month later than at the pole, on 21 September. Near the North Pole we estimate the length of the melt season is about 58 days, while at the margin of the Arctic Ocean the melt season is about 100 days.

The spring warming is associated with a lengthening of the melt season by 0.9 days/decade over the entire Arctic Ocean. The eastern Arctic Ocean shows an increasing trend of 2.6 days $(\text{decade})^{-1}$; however, the western Arctic Ocean shows a slight decreasing trend of -0.4 days $(\text{decade})^{-1}$ in the length of the melt season.

These trends are related to the changes in circulation noted by Walsh et al. (1996), Maslanik et al. (1996), and Thompson and Wallace (1998). The AO accounts for more than half of the SAT trends over Alaska, Eurasia, and the eastern Arctic Ocean but less than half over the western Arctic Ocean.

REFERENCES

Andreas, E. L, and S. F. Ackley, 1982: On the differences in ablation seasons of Arctic and Antarctic sea ice. *J. Atmos. Sci.,* **39,** 440–447.

Belousov, S. L., L. S. Gandin, and S. A. Mashovich, 1971: *Computer Processing of Meteorological Data.* Israel Program for Scientific Translations, 210 pp.

Chapman, W. L., and J. E. Walsh, 1993: Recent variations of sea ice and air temperature in high latitudes. *Bull. Amer. Meteor. Soc.,* **74,** 33–47.

Colony, R., I. Appel, and I. Rigor, 1992: Surface air temperature observations in the Arctic Basin. Tech. Memo. TM 1-92, Applied Physics Laboratory, University of Washington, Seattle, WA, 120 pp. [Available from Applied Physics Laboratory, University of Washington, Seattle, WA 98195.]

Gorschkov, S. G., Ed., 1983: *World Ocean Atlas.* Vol. 3. *Arctic Ocean,* Pergamon Press.

Jones, P. D., S. C. B. Raper, R. S. Bradley, H. F. Diaz, P. M. Kelly, and T. M. L. Wigley, 1986: Northern Hemisphere surface air temperature variations, 1851–1984. *J. Climate Appl. Meteor.,* **25,** 161–179.

——, M. New, D. E. Parker, S. Martin, and I. G. Rigor, 1999: Surface air temperature and its changes over the past 150 years. *Rev. Geophys.,* **37,** 173.

Lindsay, R. W., 1998: Temporal variability of the energy balance of thick Arctic pack ice. *J. Climate,* **11,** 313–333.

Martin, S., and E. A. Munoz, 1997: Properties of the Arctic 2-meter air temperature field for 1979 to the present derived from a new gridded dataset. *J. Climate,* **10,** 1428–1440.

——, ——, and R. Drucker, 1997: Recent observations of a spring–summer surface warming over the Arctic Ocean. *Geophys. Res. Lett.,* **24,** 1259–1262.

Maslanik, J. A., M. C. Serreze, and R. G. Barry, 1996: Recent decreases in Arctic summer ice cover and linkages to atmospheric circulation anomalies. *Geophys. Res. Lett.,* **23,** 1677–1680.

Parkinson, C. L., 1992: Spatial patterns of increases and decreases in the length of the sea ice season in the North Polar Region, 1979–1986. *J. Geophys. Res.,* **97,** 14 377–14 388.

Robinson, D. A., M. C. Serreze, R. G. Barry, G. Scharfen, and G. Kukla, 1992: Large-scale patterns and variability of snowmelt and parameterized surface albedo in the Arctic basin. *J. Climate,* **5,** 1109–1119.

Smith, D. M., 1998: Recent increase in the length of the melt season of perennial Arctic sea ice. *Geophys. Res. Lett.,* **25,** 655–658.

Thompson, D. W. J., and J. M. Wallace, 1998: The Arctic oscillation signature in the wintertime geopotential height and temperature fields. *Geophys. Res. Lett.,* **25,** 1297–1300.

Thorndike, A. S., and R. L. Colony, 1980: Arctic Ocean Buoy Program data report, 19 January 1979–31 December 1979. Polar Science Center, Applied Physics Laboratory, University of Washington, Seattle, WA, 131 pp. [Available from Polar Science Center, Applied Physics Laboratory, University of Washington, Seattle, WA 98195.]

——, and ——, 1982: Statistical properties of the atmospheric pressure field over the Arctic Ocean. *J. Atmos. Sci.,* **39,** 2229–2238.

Walsh, J. E., W. L. Chapman, and T. L. Shy, 1996: Recent decrease of sea level pressure in the central Arctic. *J. Climate,* **9,** 480–485.

Winebrenner, D. P., E. D. Nelson, R. Colony, and R. D. West, 1994: Observation of melt onset on multiyear Arctic sea ice using the ERS 1 synthetic aperture radar. *J. Geophys. Res.,* **99,** 22 425–22 441.